Available online at www.sciencedirect.com
SCIENCE DIRECT®
Journal of Power Sources 131 (2004) 313–319
JOURNAL OF POWER SOURCES
www.elsevier.com/locate/jpowsour

CFD simulation tool for solid oxide fuel cells

N. Autissier, D. Larrain*, J. Van herle, D. Favrat

Laboratory for Industrial Energy Systems (LENI), Institute of Energy (ISE), Swiss Federal Institute of Technology (EPFL), Lausanne CH-1015, Switzerland

Received 30 September 2003; accepted 6 November 2003

Abstract

A 3D simulation tool for solid oxide fuel cells is presented. The aim of this work is to predict current density, flow, temperature and concentration fields in order to compare and optimize repeat element geometry for a whole stack. A commercial CFD tool was used, solving mass, momentum and energy equations; whereas chemical kinetic equations are computed from external sub-routines. A steady-state case is presented, fed with hydrogen. The flow is laminar for both air and fuel. Radiative heat transfer is taken into account between inner surfaces. On boundaries, convective and radiative heat transfers are assumed at external surfaces between repeat element and oven. Due to the large range of dimensions (cells: 300 μm thick, gas channels: 1 mm height, whole cell: 80 mm × 80 mm) a fine mesh was needed. Data for conductivities and kinetics were estimated from experiments performed in-house. Simulation results are presented and compared to real repeat element test measurements for the current-potential characteristics.

Keywords: Sofc; Modelling; CFD; Experimental parameters

1. Introduction

At this stage of SOFC stack development, optimization of geometry is almost as crucial as material development. The geometry of a stack is complex, with manifold and gas channels distributing fuel and air among and within cells. The solid oxide fuel cell implies high operating temperature and introduces issues in thermal management. For example, the thermal behavior will influence the material stability and the response of the stack to fluctuating inlet gas compositions is not commonplace. As experiments are expensive and time consuming, there is a need for tools, to predict current densities, temperature field, pressure drop, etc.

In this paper, a computational fluid dynamics (CFD) tool is presented, allowing detailed calculations of physical phenomena. The accuracy of FLUENT^{TM}commercial software has been widely demonstrated, but as we added sub-routines to calculate reaction rates and current densities, we verified the conservation equations.

Generally, development of a new cell structure or electrode composition is performed on small active areas ($1\,cm^2$). For the stack development, larger cells are needed and power densities observed on these ($\simeq 50\,cm^2$) are far less than those on small cells. We decided to determine cell resistance and polarization losses from small cell measurements and compute the behavior for the larger geometry. Finally, we compared the simulation results with experiment on the same geometry.

2. Experimental

Cells are anode-supported, 200 μm thick with a 6–8 μm thick electrolyte layer. While developing cells for stack testing we produce mainly two sizes of cells. On the one hand, cells composed of $16\,cm^2$ of anode-supported electrolyte (ASE) with $1\,cm^2$ active cathode area are performed to measure electrochemical performances of new compositions, and for quality control of produced cells. On the other hand, $67\,cm^2$ of ASE cells with $50\,cm^2$ active area are produced to build stacks. Both sizes are produced from the same batches to ensure as much as possible identical electrochemical properties. In the present study we fed cells with hydrogen as fuel and air as oxidant to compare with the simulation, where reforming reactions have not been implemented yet. $I-V$ characteristics are recorded, at constant air and fuel flux, and for several temperatures.

* Corresponding author. Tel.: +41-21-693-53-57; fax: +41-21-693-35-02.
E-mail address: diego.larrain@epfl.ch (D. Larrain).

0378-7753/$ – see front matter © 2004 Elsevier B.V. All rights reserved.
doi:10.1016/j.jpowsour.2003.11.089

Nomenclature

C_{ij}	inertial losses coefficients
C_p	heat capacity of the mixture
D_{ij}	diffusion coefficient for species in the mixture
$D_{T,i}$	thermal diffusion coefficient
Da_{ij}	Darcy viscous losses coefficients
$\mathcal{D}_{ij}$	binary mass diffusion coefficient
E_f	total fluid energy
E_s	total solid energy
F	Faraday constant
$\vec{F}$	momentum source
ΔG_0	free Gibbs energy of formation
h_i	enthalpy of i species
I	unit tensor
j	current density
j_{leak}	leakage current density
$\vec{J}_i$	diffusion flux of species i
k_{eff}	effective thermal conductivity
M^{out}, M^{in}	mass flux in and out
P_i	partial pressure of species i
q	heat flux through boundaries
r_i	net rate of production of species i
R	universal gas constant
R_{ohm}	ohmic resistance of the electrolyte
R_{pol}	resistance for polarization losses
S^h	heat source
T	temperature
T_{out}	temperature of the outlet gas
U_{cell}	potential of the cell
U_{Nernst}	Nernst potential
U_{OCV}	cell potential in open circuit
$\vec{v}$	velocity
v_{mag}	velocity magnitude
V_i	diffusion velocity
X_i	mole fraction
Y_i	mass fraction of species

Greek letters

ε	error
γ	porosity of the medium
μ	molecular viscosity
ρ	density of the mixture
$\bar{\bar{\tau}}$	stress tensor
∇	gradient

2.1. Small cells measurements

The aim is to characterize the anode supported electrolyte (ASE) to define the model parameters. The small cell is tested in near ideal condition, with massive fuel and air flux (fuel utilization less than 10%), and platinum and nickel mesh as current collectors. $I-V$ measurements have been performed from 690 to 890 °C. Results are shown in Fig. 1.

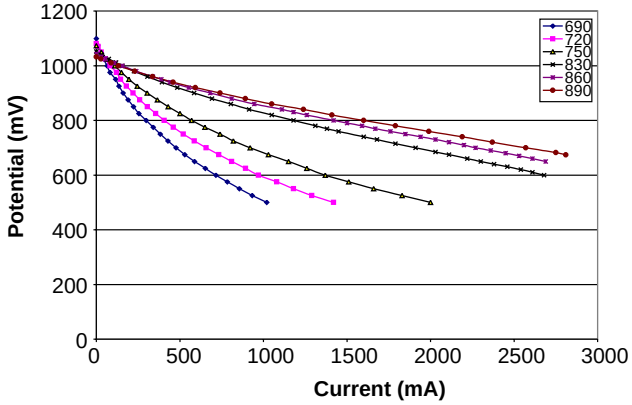

Fig. 1. Characteristic $I-V$ curves for 1 cm^2 active area button cells (16 cm^2 ASE).

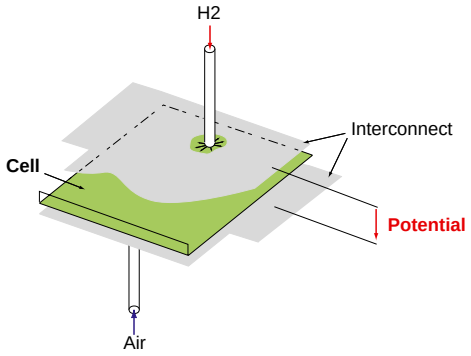

Fig. 2. Repeat element concept with internal manifolding.

2.2. Single repeat element tests

Experiments on repeat elements are based on the HTCeramix-LENI concept (see Fig. 2), with internal manifolding, on 80 mm × 80 mm anode supported cells with about 50 cm^2 of active cathode area, with gas diffusion layers on both electrodes [1]. Interconnects are formed with 0.75 mm thick metallic sheets on both sides.

The present paper discusses a single repeat element, so results with only one element in a setup are given here. The setup is placed in an electrically heated oven with a controlled temperature of 750 °C.

3. Theory

Understanding and predicting SOFC behavior implies calculating at the same time various coupled phenomena:

(1) thermal behavior, with conductive, convective and radiative heat transfer;
(2) multicomponent gas flow;
(3) electrochemical reactions, involving partial pressures, local temperature, ionic and electronic conduction.

Facing those issues we decided to use the commercial CFD tool FLUENT, able to compute the two first points above,

and added sub-routines to calculate the electrochemical part. Electrochemical behavior of the cell is experimentally fitted on small cells where we could partially uncouple the phenomena, and then applied to complex geometry.

3.1. Assumptions

For thin anode supported cells, we assume that the current paths are straight, perpendicular to the electrolyte layer [2]. At high temperature, gas mixtures can be accurately represented as mixtures of ideal gases, so heat capacities are functions of temperature only [3]. The heat capacity of the mixture is calculated with a volume-weighted mixing law of individual heat capacities. Thermal conductivities and viscosity are calculated from a mass-weighted mixing law of individual values. Individual values are calculated from a temperature-dependent polynomial curve. The cell thermal conductivity is calculated from a Ni-YSZ anode cermet formula [4].

According to Reynolds numbers, between 1 for fuel flow and 10 for air flow, the flow is assumed to be laminar. Anode support, anode active layer, electrolyte and cathode active layer are modeled as one discrete unit. Reactions are defined on each surface of this solid unit, with oxygen consumption on the cathode side, hydrogen consumption and water production on the anode side. Heats of reactions are computed and corresponding heat sources are included in the energy equation. Electric power is removed from the system.

3.2. Equations

Every equation considers the three dimensions of space and the time dimension however in the present study the steady-state condition is supposed.

The mass conservation equation includes transport phenomena, diffusion and a reactive production term.

$$\frac{\partial}{\partial t}(\rho Y_i) + \nabla(\rho \vec{v} Y_i) = -\nabla \vec{J}_i + r_i \tag{1}$$

The diffusion term is calculated from:

$$\vec{J}_i = -\sum_{j=1}^{N-1} \rho D_{ij} \nabla Y_j - D_{\mathrm{T},i} \frac{\nabla T}{T} \tag{2}$$

Diffusion coefficients are calculated from the Maxwell–Stephan equation [5]:

$$\sum_{j=1, j\neq i}^{N} \frac{X_i X_j}{\mathcal{D}_{ij}} (\vec{V}_j - \vec{V}_i) = \vec{d}_i - \frac{\nabla T}{T} \sum_{j=1, j\neq i}^{N} \frac{X_i X_j}{\mathcal{D}_{ij}} \left(\frac{D_{\mathrm{T},j}}{\rho_j} - \frac{D_{\mathrm{T},i}}{\rho_i} \right) \tag{3}$$

In the momentum conservation equation, gravitational body force was neglected (gases, forced convection, small dimensions). Pressure and stress tensor work terms are calculated with an additional source term $\vec{F}$, for a simulated porous medium:

$$\frac{\partial}{\partial t}(\rho \vec{v}) + \nabla(\rho \vec{v} \vec{v}) = -\nabla p + \nabla(\bar{\bar{\tau}}) + \vec{F} \tag{4}$$

with

$$\bar{\bar{\tau}} = \mu[(\nabla \vec{v} + \nabla \vec{v}^{\mathrm{T}}) - \tfrac{2}{3} \nabla \vec{v} I] \tag{5}$$

To model the gas diffusion layers, we assumed a porous medium between the cell and the interconnects. The porous media is then modeled as a sink in the momentum equation:

$$F_i = -\left(\sum_{j=1}^{3} \mathrm{Da}_{ij} \mu v_j + \sum_{j=1}^{3} C_{ij} \frac{1}{2} \rho v_{\mathrm{mag}} v_j \right) \tag{6}$$

The energy equation is computed from a porosity weighted composite of energy equations of the solid and fluid phase:

$$\frac{\partial}{\partial t}(\gamma \rho_{\mathrm{f}} E_{\mathrm{f}} + (1-\gamma)\rho_{\mathrm{s}} E_{\mathrm{s}}) + \nabla(\vec{v}(\rho_{\mathrm{f}} E_{\mathrm{f}} + p)) = \nabla \left[k_{\mathrm{eff}} \nabla T - \left(\sum_i h_i J_i \right) + (\bar{\bar{\tau}} \vec{v}) \right] + S_{\mathrm{f}}^{\mathrm{h}} \tag{7}$$

3.3. Reaction rate

In the present case, the fuel is hydrogen and the oxidant is air so the overall reaction is:

$$\mathrm{H_2} + \tfrac{1}{2}\mathrm{O_2} \rightarrow \mathrm{H_2O} \tag{8}$$

The reaction rate $r_{\mathrm{H_2O}}$ depends on current density j:

$$r_{\mathrm{H_2O}} = \frac{j}{2F} \tag{9}$$

A simple semi-empirical reaction rate is used:

$$U_{\mathrm{cell}} = U_{\mathrm{Nernst}} - (R_{\mathrm{ohm}} + R_{\mathrm{pol}}) j \tag{10}$$

$$U_{\mathrm{Nernst}} = \frac{-\Delta G_0}{2F} + \frac{RT}{2F} \ln \left(\frac{P_{\mathrm{O_2}}^{1/2} P_{\mathrm{H_2}}}{P_{\mathrm{H_2O}}} \right) \tag{11}$$

The polarization resistance can be calculated from measurements. On small cells tests, fuel is in excess so that partial pressures in Eq. (11) could be considered as constant. A resistance function, depending on temperature and local current is determined. We fitted the resistance with a temperature and current dependent law. The numerical values are available in Table 1.

$$R_{\mathrm{pol}} = A(T) j^{B(T)} \tag{12}$$

$$A = a_1 \times T^2 + a_2 \times T + a_3$$
$$B = b_1 \times T^2 + b_2 \times T + b_3$$

Table 1
Numerical values

	a	b
1	4.016E−04	−3.283E−06
2	−8.509E−01	5.717E−03
3	4.399E02	−2.792E00

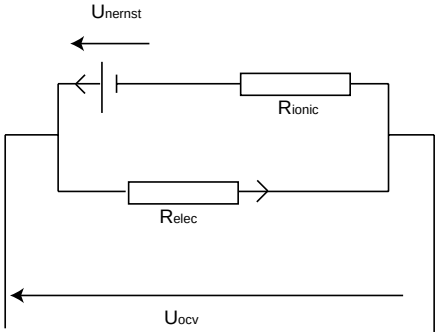

Fig. 3. equivalent electric scheme.

A constant ohmic resistance ($R_{ohm} = 0.23\,\Omega/cm^2$) is added to the resistance measured on small cells, to take into account the gas diffusion layer and the interconnect electrical resistance.

With the ASE concept, the electrolyte can be very thin, in our case between 5 and 10 μm.

In this case, the electrolyte can be doped throughout by impurities, causing electronic conduction increase and leakage current. Electronic conduction in one direction allows ionic conduction in the other [6]. This implies a modified open circuit voltage. The phenomenon is added in the model. The circuit was modified, adding an electronic conduction path for the electrolyte [7]. This configuration is shown in Fig. 3. Leakage currents depend on the ionic and electronic conductivity. Those values were estimated [8] from experimental OCV values at several temperatures, Eq. (10) leads to (13):

$$U_{cell} = U_{OCV} - (R_{ohm} + R_{pol})\,j \tag{13}$$

At open circuit, ionic current is equal to electronic current:

$$U_{OCV} = U_{Nernst} - R_{ionic}\,j_{leak} \tag{14a}$$

$$j_{leak} = \frac{U_{OCV}}{R_{electronic}} \tag{14b}$$

3.4. Boundary conditions

The cell exchanges heat by conduction with the test set-up (metal flanges), the setup is placed in an oven and exchanges heat with the environment. This exchange is driven by two phenomena: natural convection within the gas of the oven and radiation between inner surfaces. In the laboratory test setup, unreacted fuel is burned right outside the cell with oxygen from the environment. This post-combustion zone creates a higher temperature heat exchange with the corresponding side. Calculating combustion rates implies a fine meshed zone. In the present model, we simplified the phenomenon by fixing a combustion temperature. A more detailed model with a meshed post-combustion zone is in elaboration at this time and will be presented in future. As the meshed volume stops at the outlet of the stack, we could not calculate species back-diffusion through those boundaries. We will notice consequences of this assumption further on.

3.5. Numerical aspects

Each of the previous equations, including the reaction rates, are solved at each iteration. The mesh was created with GAMBIT preprocessing software. The model includes interconnects, gas diffusion layers and the cell. The entire meshed volume is divided in about 100,000 cells (see Fig. 4), with variable sizes depending on location. Because of a symmetry plane in the geometry, only half of the volume is meshed. Mesh dimensions follow real experimental sizes except for interconnects thicknesses (1 mm) in the model where experimental interconnects are 0.75 mm thick. The model yields results for a set of boundary conditions in about 150 iterations and 10 min.

3.6. Validation

As functions for the reaction rates, species consumption, heat sources and sinks were defined, we verified the mass and energy balances.

The mass balance between inlet and outlet mass fluxes amounted to:

$$\sum M^{in} - \sum M^{out} = \varepsilon_{mass}, \qquad \varepsilon_{mass} \le 1.5 \times 10^{-12}\,\text{kg/s} \tag{15}$$

The energy balance between heat fluxes through outer solid surfaces, energy fluxes through inlet and outlets by transport phenomena, heats of reaction and electric power amounted to:

$$\begin{aligned} &\sum q - \sum M^{out} H_{out} + \sum M^{in} H_{in} + U_{cell} I = \varepsilon_{energy}, \\ &\qquad \varepsilon_{energy} \le 2.8 \times 10^{-3}\,\text{W} \\ &I = \textstyle\int_S j\,\mathrm{d}S \\ &H = \textstyle\sum_{species} \Delta_f h_i^0 + \int_{T_0}^{T} C_p\,\mathrm{d}T \end{aligned} \tag{16}$$

We can conclude that the sub-routines are consistent with conservation equations and that the model is numerically verified.

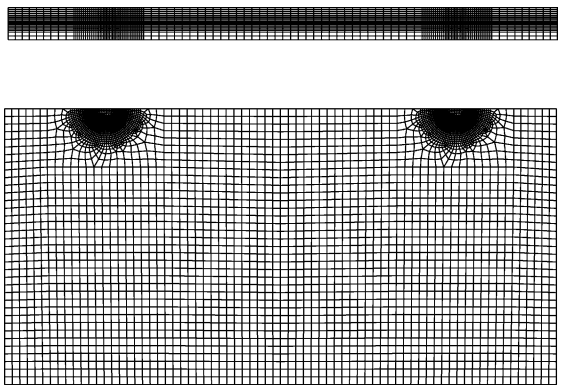

Fig. 4. In-plane and vertical cut of the mesh.

4. Results and discussion

Characteristic $I - V$ curves have been simulated to compare with experimental values (Figs. 5 and 6). Besides the general trend of the curves, we noticed a shift of the experimental curve, of about −20 mV; the experimental open circuit voltage is still lower than the calculated one. We explain this phenomenon by omitting in the model to calculate

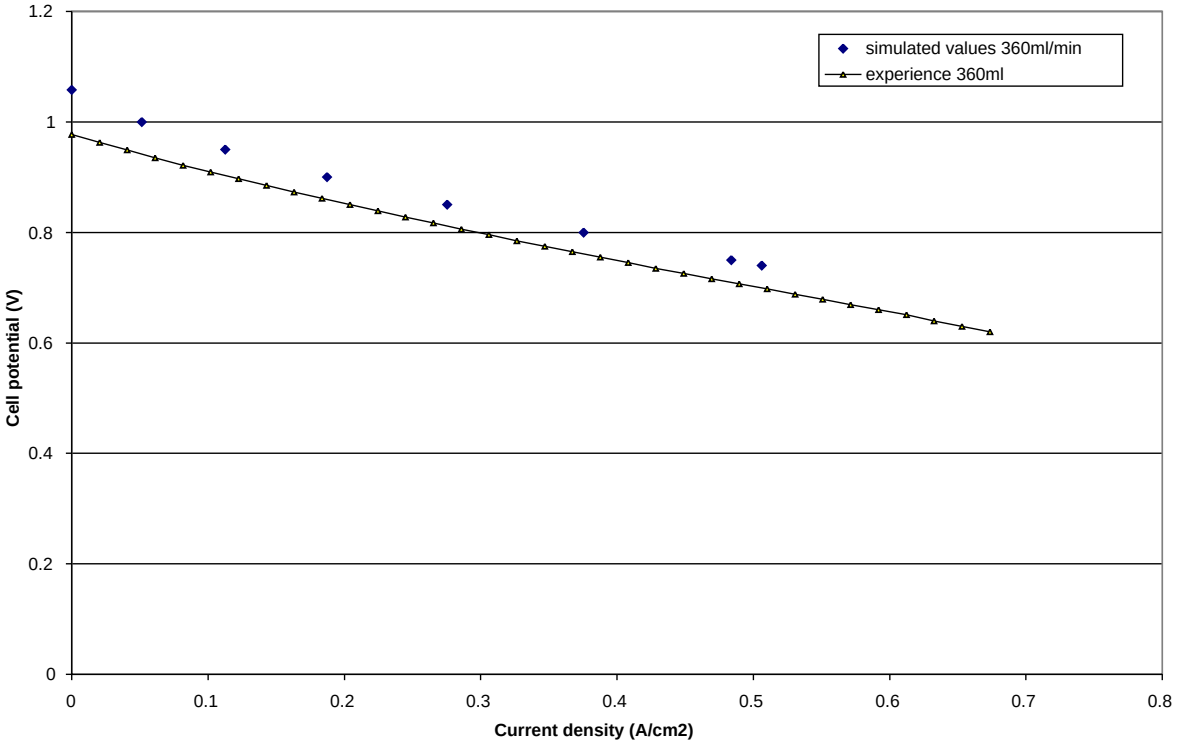

Fig. 5. Cell potential depending on current density, H_2 flux 360 ml/min, air flux 2 l/min, 50 cm^2 active area.

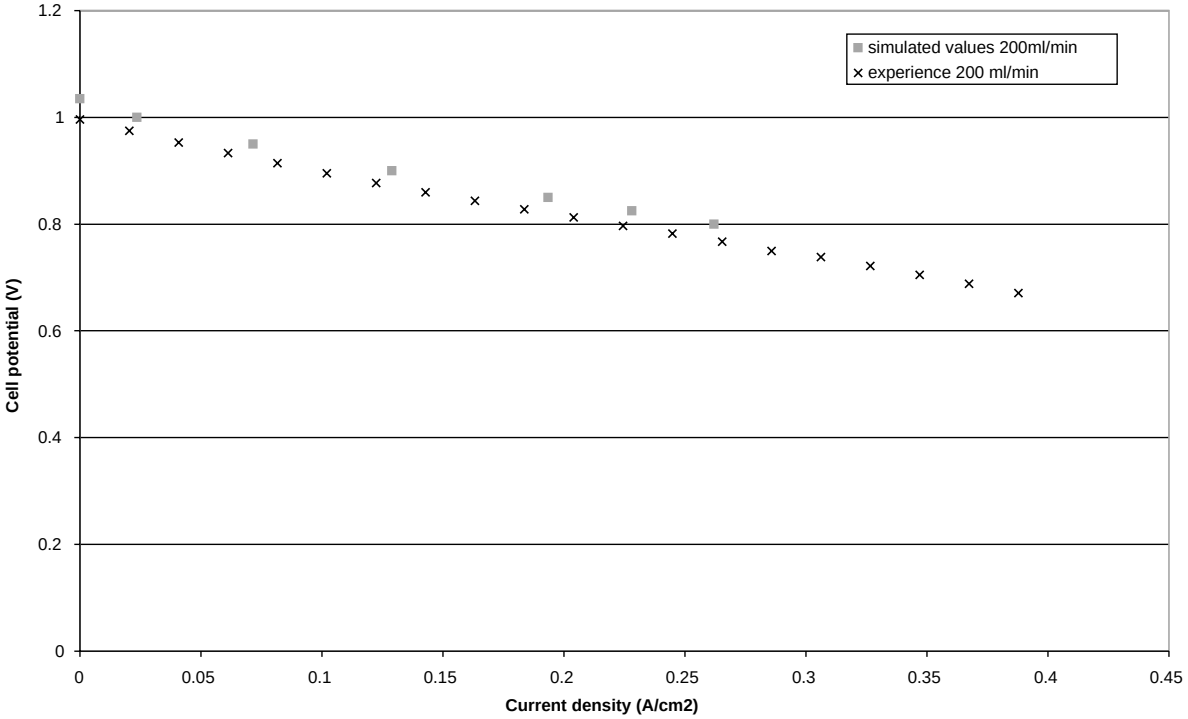

Fig. 6. Cell potential depending on current density; 200 ml/min H_2, $\lambda = 2.5$.

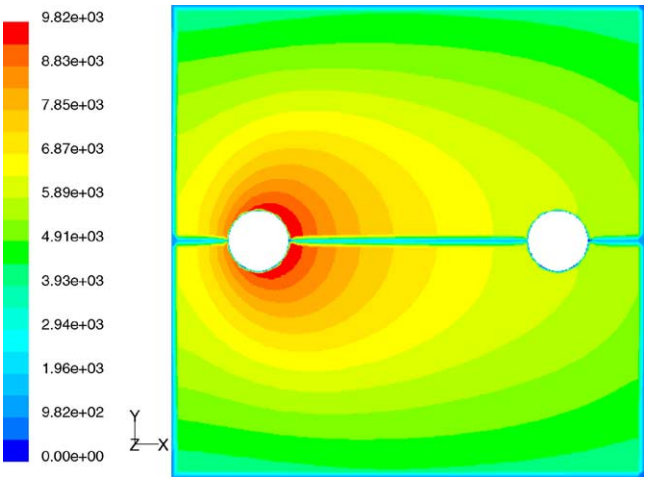

Fig. 7. Current density on the cell (A/m^2) @0.7 V and 28.8 A; @40% fuel utilization.

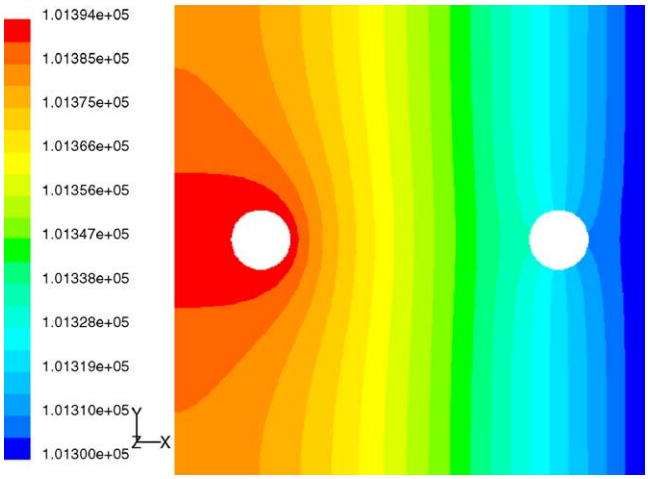

Fig. 9. Pressure field in anode side.

back-diffusion through outlets, which modify partial pressure near the outlet and thus the OCV. This diffusion could lead to the observed loss.

Comparing small cell results to repeat element results, a strong difference is apparent. Average current densities on large repeat elements are only half of those on small cells, at the same potential. For a large part, this is assigned to the geometrical effect. As the partial pressure of hydrogen decreases, Nernst potential decreases. Fig. 7 shows current density distribution for the repeat element fed with 360 ml/min hydrogen and an air excess ratio of 2.5. Near the fuel entrance (Fig. 7), the large cell produces locally around 1 A cm^{-2}, which can be compared to small cells results. Large areas close to the walls encounter low hydrogen partial pressure due to lower local flow rate (Fig. 8).

Adequate geometrical design is therefore paramount. To increase average current density, effort has to be put in cell and stack shaping. In this case, a strong limitation of performance arise from geometry: this limitation is not explained by electrochemical performance but by a non homogeneous supply of reactants on the surface.

The fine mesh of the model allows to compute the pressure field so as to predict pressure drop for complex manifold, depending on temperature gas velocity and composition. Fig. 9 shows an example of the pressure results obtained.

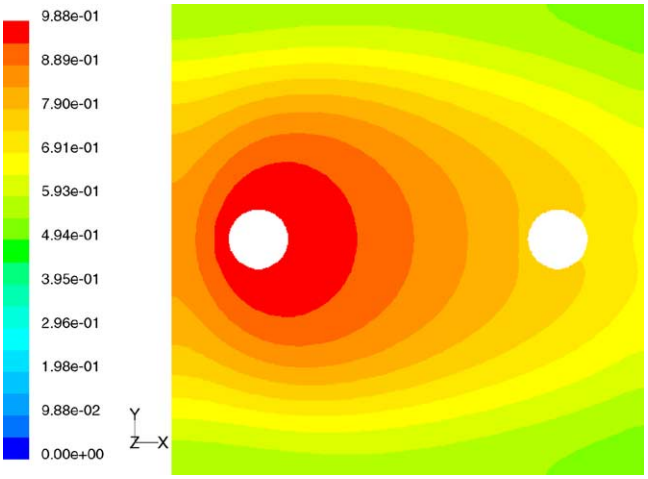

Fig. 8. Hydrogen molar fraction @0.7 V and 28.8 A; @60% fuel utilization.

5. Conclusion

A modeling tool has been developed and validated to compute complex flow fields in SOFC repeat elements, with detailed geometry. Good accuracy has been demonstrated between simulations and experimental results.

The methodology employed is as follows.

(1) Electrochemical characterisation of ASE, defining the performance within a range of temperature and current. This experimental work is done on small cells.
(2) Modelling the real geometry of the large cell design to predict power and behavior.
(3) Optimize and modify the geometry in order to increase performance, and avoid poor concentration regions.

An explanation of the lower power density obtained on a repeat element compared to a small cell was given. These results have shown that cell performance can be improved by better flow design. The need for optimization in the geometrical domain arises, with multiple criteria such as power density, temperature gradients or chemical stability. In further developments, the post-combustion zone will be simulated to study the interaction with the cell such as heat exchange or species back-diffusion through the outlet. No further development of the model is needed for studying transient behavior as the software is already designed for it. As the type of fuel is a key issue for fuel cells, internal

reforming aspects of various fuels will be studied adding subroutines for chemical behavior.

Acknowledgements

This work was supported by the Swiss Federal Energy Office (contract 86894) and the Swiss National Science Foundation (contract 200021-100721/1). Thanks to M. Molinelli for repeat element testing.

References

[1] M. Molinelli, D. Larrain, R. Ihringer, N. Autissier, O. Bucheli, J. Van herle, D. Favrat, Current collection and stacking of anode supported cells with metal interconnects to compact repeating units, in: S.C. Singhal, M. Dokiya (Eds.), SOFC VIII, The ElectroChemical Society, July 2003, pp. 905–913.
[2] E. Fontes, Current and potential distribution in gas diffusion electrode, in: J. Huijsmans (Ed.), Fifth European Solid Oxide Fuel Cell Forum, July 2002, pp. 937–944.
[3] B. Todd, B. Young, Thermodynamic and transport properties of gases for use in solid oxide fuel cell modelling, J. Power Sources 110 (2002) 186–200.
[4] T. Kawashima, M. Hishinuma, Thermal properties of porous Ni/YSZ particulate composites at high temperatures, Mater. Trans. JIM 37–39 (1996) 1518–1524.
[5] H.J. Merck, The macroscopic equations for simultaneous heat and mass transfert in isotropic, continuous and closed systems, Appl. Sci. Res. (8) (1958) 73–99.
[6] R. Ihringer, Electrolytes minces sur supports anode dans les piles à combustibles SOFC, Ph.D. thesis, EPFL, 2001.
[7] K. Chen, An electrolyte model for ceramic oxygen generator and solid oxide fuel cell, J. Power Sources 111 (2002) 320–328.
[8] D. Larrain, Generalised model of planar SOFC repeat element for design optimization, J. Power Sources, 2003, submitted for publication.